



Contents lists available at ScienceDirect

International Journal of Plasticity

journal homepage: www.elsevier.com/locate/ijplas

Emission of dislocations from nanovoids under combined loading

Vlado A. Lubarda*

Department of Mechanical and Aerospace Engineering, University of California, San Diego, La Jolla, CA 92093-0411, USA
 Montenegrin Academy of Sciences and Arts, Rista Stijovića 5, 81000 Podgorica, Montenegro

ARTICLE INFO

Article history:

Received 21 December 2009

Received in final revised form 3 April 2010

Available online 20 April 2010

Keywords:

Core cut-off

Critical stress

Dislocation emission

Nanovoid

Slip plane

ABSTRACT

Among all directions available for dislocation emission from the surface of a cylindrical circular void, the direction of the most likely emission is determined. It is shown that this direction is different from the direction of the maximum shear stress at the surface of the void due to the applied loading. The critical stress and the direction of the dislocation emission are determined for circular nanovoids under remote uniaxial, pure shear, and arbitrary biaxial loading. The analysis includes effects of the loading orientation relative to the discrete slip plane orientation. It is shown that dislocations are emitted more readily from larger nanovoids and that wider dislocations are emitted under lower applied stress than narrow dislocations. Different mechanisms, under much lower stress, operate for growth of the micron-size voids.

© 2010 Elsevier Ltd. All rights reserved.

1. Introduction

The void growth in ductile materials and the material failure preceded by the void coalescence have been studied over a long period of time by using both analytical and computational means. The survey of the work based on continuum plasticity can be found in Tvergaard (1990). The analysis of void growth and coalescence in single crystals by crystal plasticity models was performed by Quinn et al. (1995), Ohashi (2005), Potirniche et al. (2006a), Liu et al. (2007), and others. The strain gradient theories of polycrystalline and single crystal plasticity were also used to evaluate the effect of the void size on its growth (e.g., Huang et al., 2004; Tvergaard and Niordson, 2004; Liu et al., 2005; Wen et al., 2005; Li and Steinmann, 2006; Borg et al., 2008). Another recently employed approach to the study of void growth in ductile materials is based on discrete dislocation dynamics (Huang et al., 2007; Hussein et al., 2008; Segurado and Llorca, 2009, 2010). In these two-dimensional simulations, it is assumed that the dislocation loops (the pairs of opposite-signed edge dislocations) are nucleated at random sites along the slip planes when the magnitude of the local resolved shear stress exceeds a critical value over a nucleation period of time. Once generated, dislocations glide along their slip planes, interact, possibly annihilate, pileup, and exit at the free surface of the void causing the expansion of the void. One important result of this study is that the rate of growth is smaller for smaller voids (“smaller is slower”). There has also been a significant amount of work devoted to the study of nanovoid growth in single crystals by molecular dynamics simulations (Farrissey et al., 2000; Rudd and Belak, 2002; Seppälä et al., 2004; Marian et al., 2005; Song et al., 2006; Rudd et al., 2007; Zhu et al., 2007; Potirniche et al., 2006b; Traiviratana et al., 2008; Meyers et al., 2009; Rudd, 2009). One outcome of these studies is that the stress required for void growth by dislocation emission is significantly larger for nanovoids than for larger voids (“smaller is stronger”).

In this paper, we use a two-dimensional model of the emission of edge dislocations from a cylindrical void, introduced by Lubarda et al. (2004), to perform an analytical study of the process based on a closed form solution for the Volterra

* Address: Department of Mechanical and Aerospace Engineering, University of California, San Diego, La Jolla, CA 92093-0411, USA. Tel.: +1 858 534 3169; fax: +1 858 534 5698.

E-mail address: vlubarda@ucsd.edu

dislocation near a circular void under plane strain conditions. Although simplified, this model is able to deliver good estimates of the critical stress required for the onset of dislocation emission. The model also provides a simple geometric description of the mechanism of material transport from the surface of the void, which gives rise to its growth. This takes place by the emission of multiple dislocation dipoles, each of which consisting of a positive and negative edge dislocation, residing one above another on two parallel slip planes. The material associated with the creation of such dipole is supplied by the expansion of the void and the corresponding outward transport of the material from its surface. There is no analytical solution for the stress field around a dislocation semi-loop or a loop segment,¹ being emitted from the surface of a spherical or rounded void, but this three-dimensional dislocation emission process has been extensively studied by the MD or hybrid MD/FEM techniques. Upon initial emission of loop segments on different slip planes, the curved segments expand and interact with each other. After cross slip at the slip plane intersections and annihilation of the touching dislocation screw segments, the closed prismatic loops form, which consist of loop segments on different slip planes. These prismatic loops glide away, carrying the material away from the void causing it to grow. For example, if the area within a plane dislocation loop is A_0 , the volume $A_0 b$ of the material has been transported from the surface of the void, where b is the component of the Burgers vector of the dislocation orthogonal to the plane of the loop. This has been recently discussed in great detail for both fcc and bcc metals by Rudd et al. (2007) and Rudd (2009). They have shown that main differences in the process of void growth and shape change in these metals come from the fact that fcc metals have lower lattice friction stress (once a dislocation is punched out, there is a little lattice resistance to its further glide), and lower stacking fault energy, so that dislocations tend to split into their partials with the ribbons of stacking faults in-between them.

There are three main objectives of this paper. The first is to improve the analysis of Lubarda et al. (2004), which was based on the assumption that the dislocation is emitted from the surface of the void along the direction of the maximum shear stress. In Section 2, we show that the dislocation is more readily emitted along other directions, which may be quite different from the 45° direction corresponding to the maximum shear stress at the surface of the void. The critical stress for the dislocation emission along these directions is found to be higher than earlier reported values. We also point out a subtle point about the expression for the image force on the dislocation exerted by the surface of the void, which is associated with a non-uniqueness of the solution for the stress field around the Volterra dislocation in multiply connected regions. The second objective of the paper is to extend the previous analysis to encompass other than isotropic loading conditions, i.e., to address the dislocation emission from the surface of a void under uniaxial, pure shear, and arbitrary biaxial loadings. The critical stress required for dislocation emission and the direction of this emission are determined in Section 3 for each type of the considered loading. As expected from the consideration of the stress concentration factor, the remote shear loading emits the dislocation most readily. The third objective of the present work is to incorporate in the analysis the effects of the loading orientation relative to the discrete lattice (slip plane) orientation. In Section 4, we determine the most favorable slip plane for dislocation emission and calculate the corresponding critical stress for this emission. It is shown that dislocations are emitted more readily from larger nanovoids and that wider dislocations are emitted under lower applied stress than narrow dislocations. A different mechanism operates for the growth of the micron-size voids, which dominantly takes place by sinking of the pre-existing or newly created dislocations or their segments at the surface of the void, under a far lower level of the applied stress (Segurado and Llorca, 2009). Concluding remarks are given in Section 5.

2. Dislocation emission under equal biaxial stress

Fig. 1 shows a cylindrical void of radius a in an infinitely extended isotropic homogeneous material, subjected to remote equal biaxial state of stress $\sigma_x = \sigma_y = \sigma$. Elastic deformation under plain strain conditions are assumed, so that $\sigma_z = \nu(\sigma_x + \sigma_y)$, where ν is Poisson's ratio. The inplane elastic stress field around the void (without the dislocation) is the sum of the isotropic tension $\sigma_r = \sigma_\phi = \sigma$ and the pure shear state of stress $\sigma_r = -\sigma_\phi = -\sigma a^2/r^2$, so that (Timoshenko and Goodier, 1970)

$$\sigma_r = \sigma \left(1 - \frac{a^2}{r^2}\right), \quad \sigma_\phi = \sigma \left(1 + \frac{a^2}{r^2}\right), \quad \sigma_{r\phi} = 0. \quad (1)$$

The polar coordinates r and ϕ can be expressed in terms of the polar coordinates ρ and θ , emanating from the surface of the void (Fig. 1), such that $\theta = \text{const.}$ defines a slip plane of a dislocation considered in Section 2.1. The relationships are

$$r^2 = a^2 + \rho^2 + 2a\rho \cos \theta, \quad \tan \phi = \frac{\rho \sin \theta}{a + \rho \cos \theta}. \quad (2)$$

The shear stress $\tau^a = \sigma_{\rho\theta}$ along the slip plane is determined from the stress components σ_r and σ_ϕ by using the transformation $\tau^a = -0.5(\sigma_r - \sigma_\phi) \sin 2(\theta - \phi)$. By substituting (1), this gives

$$\tau^a = \sigma \frac{a^2}{r^2} \sin 2(\theta - \phi). \quad (3)$$

The superscript a is attached to indicate that this shear stress is due to the applied stress σ . The solid curve in Fig. 2 represents the variation of the shear stress τ^a/σ with the angle θ due to applied stress $\sigma = 0.125G$, at distance $\rho = 1.5b$ from the void (b is

¹ Elastic interaction between a circular prismatic dislocation loop and a spherical cavity has been studied by Wolfer and Drugan (1988).

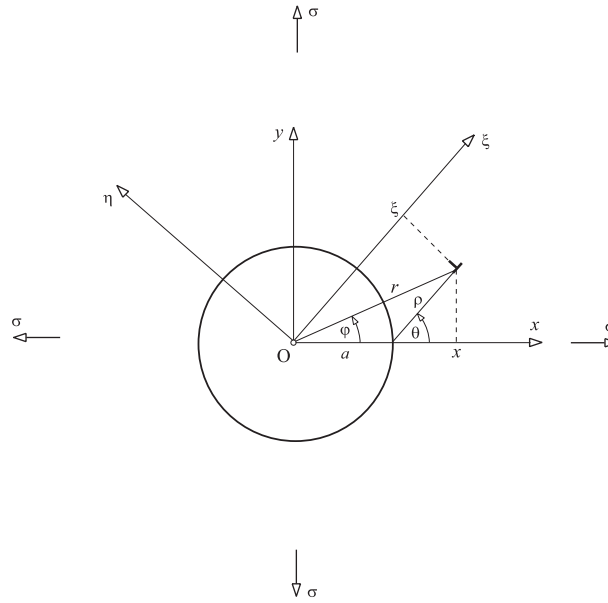


Fig. 1. Dislocation emitted from the surface of the void under remote equal biaxial tension σ . The two sets of polar coordinates (r, φ) and (ρ, θ) specify the position of the dislocation relative to the center of the void and the point on the surface of the void, respectively.

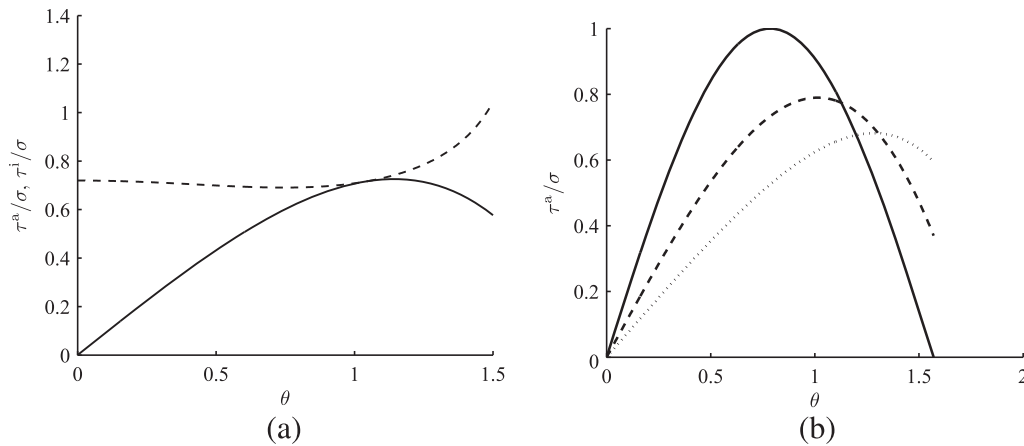


Fig. 2. (a) The solid curve is the shear stress τ^a/σ due to applied stress $\sigma = 0.125G$ vs. the angle θ , when the dislocation is at the distance $\rho = 1.5b$ from the void. The dashed curve is the magnitude of the shear stress τ^i/σ due to attraction exerted on the dislocation by the surface of the void. The two stresses balance each other at $\theta = 59.3^\circ$. (b) The shear stress τ^a/σ vs. the angle θ , at the distance: $\rho = 0$ (solid), $\rho = b$ (dashed), and $\rho = 2b$ (dotted curve) from the void. Greater the value of ρ , further is the maximum shear stress direction away from the angle $\theta = 45^\circ$ (corresponding to $\rho = 0$).

the magnitude of the Burgers vector of the dislocation, and G is the shear modulus of the material). The dashed curve is the magnitude of the shear stress τ^i/G due to attraction exerted on the dislocation by the surface of the void, determined from the expression F^i/b , which is derived in the next section.

2.1. Glide force on a dislocation near the void

Suppose that an edge dislocation is emitted from the surface of the void and that it is in the position shown in Fig. 1. The dislocation is attracted by the surface of the void along the slip plane of the dislocation by the image force $F^i = \tau^i b$, where τ^i is the shear stress at the place of the dislocation exerted by the free surface of the nearby void. By using the results for the stress fields of the Volterra dislocation near the surface of a circular void, it can be shown (see Appendix A) that

$$F^i = \frac{Gb^2 \cos(\theta - \varphi)}{2\pi(1 - \nu)} \frac{a^2}{r^3} \left(2 \frac{r^2 - a^2}{r^2} \sin^2 \theta - \frac{r^2}{a^2} \frac{r^2}{r^2 - a^2} \right). \tag{4}$$

This force corresponds to the imposed displacement discontinuity along the cut from the surface of the void to the center of the dislocation. The expression for the image force derived by Dundurs and Mura (1964) corresponds to the displacement discontinuity along the cut from the center of the dislocation to infinity. This was not noted in the earlier work by Lubarda et al. (2004), Song et al. (2006), and Traiviratana et al. (2008), who used the Dundurs and Mura expression for the image force, rather than (4). The two expressions for the dislocation force are different, the attraction being stronger in the case of the cut between the void and the dislocation (Lubarda, submitted for publication), because the stress field around dislocation in a multiply connected region depends on the cut along which the displacement discontinuity is imposed. This cut dependence was originally pointed out for screw dislocations by Lubarda (1999), and elaborated upon by Lubarda and Markenscoff (2003). Since the Volterra model was utilized in deriving (4), this expression is appropriate for a dislocation sufficiently away from the surface of the void (i.e., at the distances greater than a dislocation cut-off radius, to be discussed later in this paper).

If the remote applied stress around the void is a biaxial tension σ , its contribution to the dislocation glide force is specified by the Peach–Koehler expression $F^a = \tau^a b$. In view of (3), this is

$$F^a = \sigma b \frac{a^2}{r^2} \sin 2(\theta - \varphi). \quad (5)$$

The total glide force on the dislocation, driving it out of the void, is then $F = F^a + F^i$. By using (4) and (5), this gives

$$F = \sigma b \frac{a^2}{r^2} \sin 2(\theta - \varphi) + \frac{Gb^2 \cos(\theta - \varphi)}{2\pi(1 - \nu)} \frac{a^2}{r^3} \left(2 \frac{r^2 - a^2}{r^2} \sin^2 \theta - \frac{r^2}{a^2} \frac{r^2}{r^2 - a^2} \right). \quad (6)$$

The variation of the normalized force F/Gb with the dislocation position ρ/b in the case $a/b = 5$, $\nu = 1/3$, $\theta = 59.3^\circ$, and $\sigma = 0.125G$ is shown in Fig. 3 by the solid curve. The repulsive portion of the force due to the applied stress is shown by the dashed curve; the attractive portion due to void's free surface is shown by the dotted curve.

2.2. An analysis of the dislocation emission

In the equilibrium dislocation position, the attraction from the void is balanced by the applied stress. Thus, the condition $F = 0$ in (6) gives

$$\sigma r \sin(\theta - \varphi) = \frac{Gb}{4\pi(1 - \nu)} \left(\frac{r^2}{a^2} \frac{r^2}{r^2 - a^2} - 2 \frac{r^2 - a^2}{r^2} \sin^2 \theta \right). \quad (7)$$

Adopting the criterion from Lubarda et al. (2004), it is assumed that the dislocation will be emitted from the surface of the void if its equilibrium distance ρ from the surface of the void is equal to the dislocation core cut-off radius ρ_0 (one half of the dislocation width, which represents the extent of the dislocation core spreading). For example, if a Peierls semi-discrete model of a lattice dislocation is adopted, the core cut-off of an isolated edge dislocation is $\rho_0 = d/2(1 - \nu)$, where d is the atomic interplanar separation across the slip plane. Physically, the length ρ_0 represents the distance from the center of the dislocation at which the slip discontinuity reaches half of the maximum slip. Other definitions of ρ_0 are also possible (Lubarda and Markenscoff, 2006, 2007). In the present study, we consider the core cut-off to be the minimum distance of the center of the dislocation from the surface of the void for which the image force on the dislocation, calculated from linear elasticity and the Volterra dislocation model, is a reliable measure of the dislocation attraction to the void by its free surface.

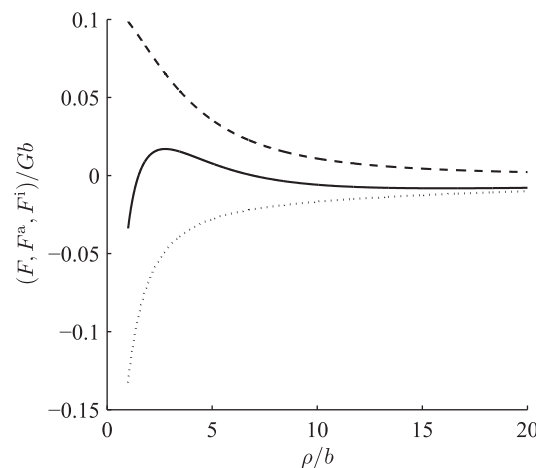


Fig. 3. The repulsive portion (F^a) of the force due to applied stress (dashed curve), the attractive portion (F^i) due to the surface of the void (dotted curve), and their sum giving the total force F (solid curve) vs. the dislocation position ρ/b . The plots are for $a/b = 5$, $\nu = 1/3$, $\theta_{cr} = 59.3^\circ$, and $\sigma = 0.125G$ (corresponding to equilibrium dislocation position at $\rho = 1.5b$).

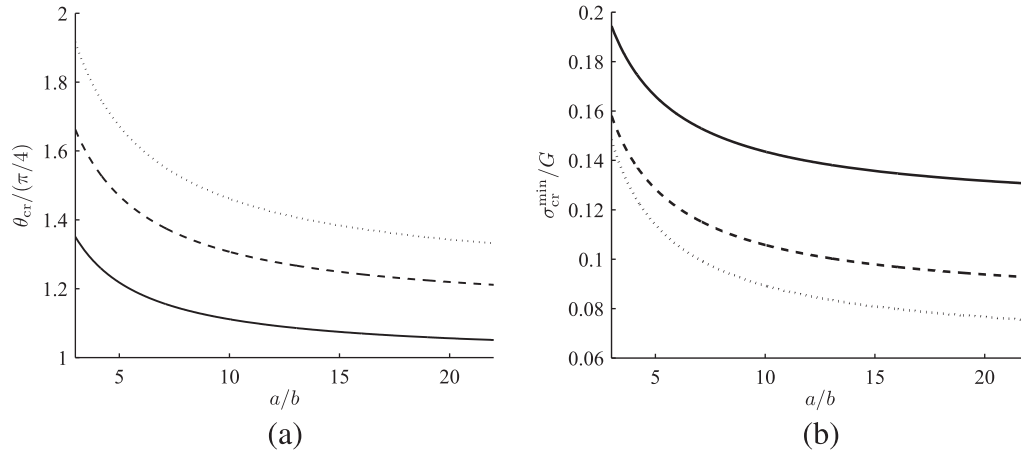


Fig. 4. (a) The effect of the void size a/b on the critical angle θ_{cr} (scaled by $\pi/4$) for the three selected values of the dislocation core radius ρ_0 . For large values of a/b , the critical angle $\theta_{cr} \rightarrow \pi/4$. (b) The minimum critical stress σ_{cr}^{min}/G required for dislocation emission vs. the ratio a/b . The solid curves are for $\rho_0 = b$, the dashed curves for $\rho_0 = 1.5b$, and the dotted curves for $\rho_0 = 2b$. Poisson's ratio is taken to be $\nu = 1/3$.

The applied stress required to keep the dislocation in equilibrium at the distance greater than ρ_0 is smaller than the stress required to keep it in equilibrium at the distance equal to ρ_0 , and thus we propose that this maximum stress value is the critical stress required for the dislocation emission. We do not consider in the present analysis the movement of the dislocation for $\rho < \rho_0$, where an incipient (incomplete) dislocation is created near the void, characterized by a strongly nonlinear slip discontinuity across the glide plane.² Consequently, by setting $\rho = \rho_0$ in (7) specifies the stress required to emit the dislocation from the surface of the void. In view of (2), this yields the following expression for the critical stress:

$$\sigma_{cr} = \frac{Gb/a}{4\pi(1-\nu)} \left(\frac{r_0^2}{a^2} \frac{1}{f_0} - 2f_0 \right), \tag{8}$$

where

$$f_0 = \frac{r_0^2 - a^2}{r_0^2} \sin \theta, \quad r_0^2 = a^2 + \rho_0^2 + 2a\rho_0 \cos \theta. \tag{9}$$

A lower stress would suffice to keep the dislocation in the equilibrium at the distance greater than ρ_0 , i.e., the equilibrium position of the dislocation is unstable, and the dislocation would be driven away from the void indefinitely, or until it is blocked by an obstacle.

The angle $\theta = \theta_{cr}$ at which the dislocation is emitted from the surface of the void corresponds to the minimum value of the applied stress, σ_{cr}^{min} , and is therefore obtained numerically as the point on the contour plot $z = 0$, obtained from the minimization condition $d\sigma_{cr}/d\theta = 0$, which gives

$$z = 2a\rho_0 f_0 \sin \theta + (r_0^2 + 2a^2 f_0^2) \frac{df_0}{d\theta} = 0, \tag{10}$$

where

$$\frac{df_0}{d\theta} = \left(1 - \frac{a^2}{r_0^2} \right) \cos \theta - \frac{2a^3 \rho_0}{r_0^4} \sin^2 \theta.$$

The contour plots $z = 0$ for the three selected values of the dislocation core radius are shown in Fig. 4a. The plots reveal the effect of the void size a/b on the critical angle θ_{cr} (scaled by $\pi/4$) at which the dislocation is emitted. Smaller the void, more pronounced is the departure of the angle θ_{cr} from the direction $\theta = 45^\circ$ associated with the maximum applied shear stress at the surface of the void due to applied stress σ . The departure is also more pronounced for larger values of the dislocation core radius ρ_0 . Fig. 4b shows the variation of σ_{cr}^{min} with a/b for the three selected values of the ratio ρ_0/b , which is obtained numerically by substituting θ_{cr} into (8). Larger stress is required to emit the dislocation from a smaller void, and the emission is further away from the $\theta = 45^\circ$ direction, associated with the maximum shear stress direction at the surface of the void due to applied stress.³ The physical reason for $\theta_{cr} \neq 45^\circ$ is that the attraction on the dislocation from the void surface may

² An analytical study of this stage of the dislocation nucleation would, of course, be of great interest, but it is hindered by the absence of a closed form solution for the Peierls dislocation near a circular void. An analytical study of the dislocation nucleation from a crack tip within the Peierls framework was performed by Rice (1992), whose analysis eliminated the need for the introduction of the poorly defined core cut-off near the crack tip.

³ Voids with radius smaller than $3b$ are presumably beyond the reach of the employed continuum type analysis. The minimum size of the void should probably be even larger than this, possibly about $5b$, so that the ledge left at the surface of the void by emitted dislocation does not appreciably distort the circular geometry of the void, assumed in the derivation of the image force.

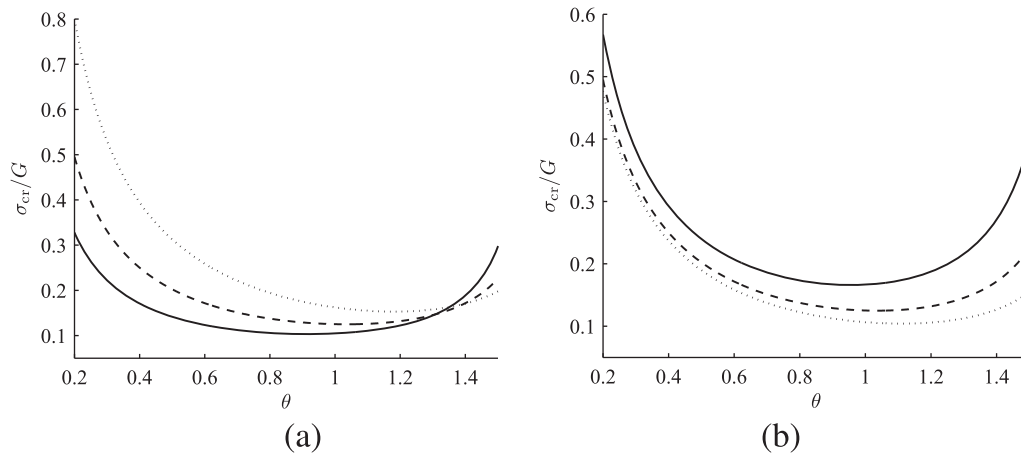


Fig. 5. The critical stress σ_{cr}/G vs. the angle θ in the case $\rho_0 = 1.5b$. (a) Solid curve: $a/b = 10$, $\sigma_{cr}^{\min} = 0.103G$, $\theta_{cr} = 52.4^\circ$; dashed curve: $a/b = 5$, $\sigma_{cr}^{\min} = 0.125G$, $\theta_{cr} = 59.3^\circ$; dotted curve: $a/b = 3$, $\sigma_{cr}^{\min} = 0.153G$, $\theta_{cr} = 67.7^\circ$. (b) The effect of the dislocation core radius ρ_0 on the critical stress, in the case $a/b = 5$. The solid curve: $\rho_0 = b$, $\sigma_{cr}^{\min} = 0.166G$, $\theta_{cr} = 54.5^\circ$; dashed curve: $\rho_0 = 1.5b$, $\sigma_{cr}^{\min} = 0.125G$, $\theta_{cr} = 59.3^\circ$; dotted curve: $\rho_0 = 2b$, $\sigma_{cr}^{\min} = 0.104G$, $\theta_{cr} = 63.6^\circ$.

be weaker at the angle different from 45° , so that in spite of the smaller resolved shear stress at that angle, the net tendency for the dislocation emission is greatest along such direction. This was not realized in the original work by Lubarda et al. (2004), who assumed that the dislocation is emitted along the direction of the maximum shear stress at the surface of the void ($\theta_{cr} = 45^\circ$), regardless of the size of the void, or the width of the dislocation.

It is noted that the cut-off radius ρ_0 appears in the denominator of the expression (8) for the critical stress. Thus, less stress is required to emit a wide dislocation (with a spread dislocation core) than a narrow dislocation, at least within our model which does not consider details of the incipient dislocation movement for $\rho < \rho_0$. This implies that dislocations are more easily emitted from voids in softer materials, which are characterized by a wider dislocation core. Furthermore, softer materials have lower lattice friction stress (Peierls stress is a decreasing function of the dislocation core width; Hirth and Lothe, 1982; Nabarro, 1997), so that once emitted dislocations will glide away through the lattice with a less resistance from it. Analytical and numerical studies suggest that reasonable estimates of the core radius are in the range from $0.5b$ to $2b$, depending on the crystalline structure (Lubarda and Markenscoff, 2007).

The curves shown in Fig. 5a are the traces of the surface $\sigma_{cr} = \sigma_{cr}(\theta, a/b)$ in the planes corresponding to different values of the ratio a/b , and for the selected value of the core radius $\rho_0 = 1.5b$. Fig. 5b illustrates the effect of the dislocation core radius on the critical stress, in the case $a/b = 5$. With the increase of the core radius, the angle θ_{cr} increases, while σ_{cr}^{\min} decreases. Some numerical values are listed in Table 1. The levels of applied stress required for dislocation emission is high (~ 0.1 – $0.2G$), but it is available under high strain rate shock loading of metals with high spall strength.

In the limit of very large voids ($a \gg b$), (8) becomes⁴

$$\sigma_{cr} = \frac{Gb/\rho_0}{4\pi(1-\nu)} \frac{1}{\sin 2\theta}, \quad \sigma_{cr}^{\min} = \sigma_{cr}(45^\circ) = \frac{Gb/\rho_0}{4\pi(1-\nu)}. \quad (11)$$

The compressive remote stress of the same magnitude would emit the positive dislocation at $\theta_{cr} = -45^\circ$. If the dislocation is the negative edge dislocation, the tensile stress would cause the emission at $\theta_{cr} = -45^\circ$, and the compressive stress at $\theta_{cr} = 45^\circ$. Similar conclusions apply to smaller voids and their corresponding values of θ_{cr} (Fig. 6).

A comment should be made regarding large values of the predicted stress required to grow a nanovoid by dislocation emission from its surface, as compared to far smaller values required to grow a micron-size or larger voids. A significantly lower stress is required to grow larger voids, because in the vicinity of such voids there are pre-existing dislocations, or their sources from which dislocations can nucleate under relatively low resolved shear stress. The void grows in this case by the exit or sink of dislocations, or their segments, at the surface of the void (Huang et al., 2007; Segurado and Llorca, 2009). For lower and medium loading rates, the void growth is also facilitated by the vacancy pipe diffusion through the cores of the dislocations (Cuitiño and Ortiz, 1996; Fisher and Antretter, 2009).

For example, in an undeformed single crystal with an initial dislocation density of the order $\rho_d = 10^{10}$ – $10^{12}/\text{m}^2$, the average dislocation spacing is about 1 – $10 \mu\text{m}$ ($\rho_d^{-1/2}$). Therefore, in the region of the radius of several microns around a nanovoid in such a crystal there are no dislocations at all, so that the only available mechanism for the void growth under dynamic loading, without sufficient time for the vacancy diffusion, is by the dislocation emission from the surface of the void. This emission may also be facilitated by the local geometric irregularities at the surface of the void.

⁴ For large voids, however, other mechanisms of the void growth prevail, which operate under far lower critical stress, as discussed below.

Table 1

The critical stress σ_{cr}^{min} and the corresponding angle θ_{cr} of dislocation emission for different void sizes and different core cut-offs. Poisson's ratio is taken to be $\nu = 1/3$. If $\nu \neq 1/3$, the listed values for σ_{cr}^{min} should be multiplied by $2/[3(1 - \nu)]$.

	$a/b = 3$	$a/b = 5$	$a/b = 10$
$\rho_0 = 1.5b$			
σ_{cr}^{min}/G	0.153	0.125	0.103
$\theta_{cr} (^{\circ})$	67.7	59.3	52.4
	$\rho_0 = b$	$\rho_0 = 1.5b$	$\rho_0 = 2b$
$a/b = 5$			
σ_{cr}^{min}/G	0.166	0.125	0.104
$\theta_{cr} (^{\circ})$	54.5	59.3	63.6

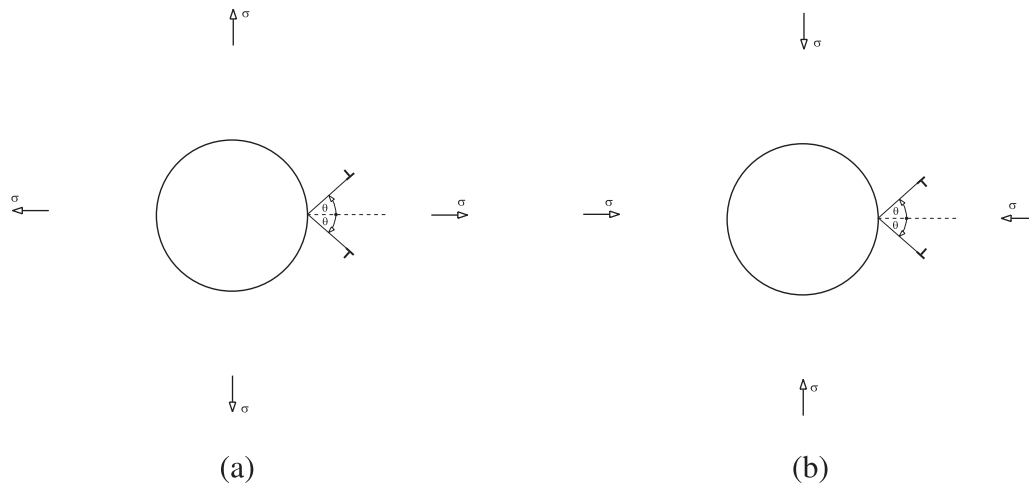


Fig. 6. Positive and negative edge dislocation emission under remote equiaxial (a) tension, and (b) compression.

It should also be pointed out that the utilized quasi-static analysis of the void growth is reasonably appropriate even for the dynamic-impact loading, because the wave front passes through the material around a nanovoid within picoseconds, leaving it in the state of nearly uniform remote stress for several nanoseconds of the duration of the pulse during which the emission of dislocations takes place.⁵

2.3. Ledge effects on the dislocation emission

The effect of the ledge left at the surface of the void behind the dislocation on the dislocation emission can be included in the analysis as follows. When the dislocation is far from the void, the ledge is fully formed with its width equal to the magnitude of the Burgers vector b . The corresponding increase of the energy is γb , where γ is the surface energy. When the dislocation is near the surface of the void, the ledge is only partially formed due to nearby dislocation core effects. Adopting the Peierls model of the dislocation, as in Lubarda et al. (2004), and the earlier work by Rice and Thomson (1974) in the context of dislocation emission from the crack tip, we assume that the width of the ledge left behind the dislocation is

$$\frac{2b}{\pi} \tan^{-1} \frac{2\rho}{e^{3/2}\rho_0}, \quad (12)$$

where e is the Neperian logarithm base. Thus, the energy increase due to the creation of the ledge is

$$U^l = \frac{2\gamma b}{\pi} \tan^{-1} \frac{2\rho}{e^{3/2}\rho_0}. \quad (13)$$

⁵ The reflected tensile pulse from the free surface of the shock-impacted Cu crystal can be of the order of $G/10$. If the duration of the pulse is $\tau = 10$ ns, its spatial length is $c\tau = 0.36 \mu\text{m}$, where $c = 3.6 \text{ km/s}$ is the longitudinal wave speed in copper.

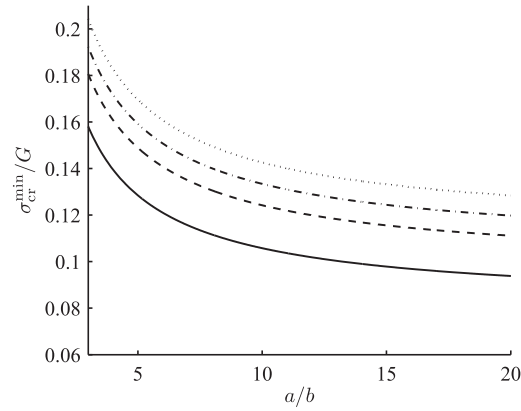


Fig. 7. The comparison of σ_{cr}^{\min} vs. a/b with and without included dislocation ledge effect, in the case $\rho_0 = 1.5b$. The solid curve is the critical stress without the ledge effect. The dashed curve corresponds to ledge parameter $\eta = 0.1$, the dashed-dotted curve to $\eta = 0.15$, and the dotted curve to $\eta = 0.2$.

The corresponding ledge force is

$$F^l = -\frac{\partial U^l}{\partial \rho} = -\frac{2\gamma}{\pi} \frac{\zeta}{\zeta^2 + (\rho/b)^2}, \quad \zeta = e^{3/2}(\rho_0/2b) \approx 2.24(\rho_0/b). \quad (14)$$

At a given temperature, the surface energy can be expressed as $\gamma = \eta Gb$, where η is a non-dimensional parameter that depends on the crystalline lattice and the strength of interatomic bonding within and across the material surface under consideration. With this representation of the surface energy, (14) becomes

$$F^l = -\frac{2\eta Gb}{\pi} \frac{\zeta}{\zeta^2 + (\rho/b)^2}, \quad (15)$$

which is independent of θ . At large $\rho \gg b$, the ledge force approaches zero, while $F^l/Gb \approx -0.284\eta b/\rho_0$ if $\rho \ll b$.

The total force F on the dislocation is the sum of (6) and (15), and in the equilibrium dislocation position $F = 0$. As in Section 2.2, it is assumed that dislocation will be emitted from the surface of the void if its equilibrium distance from the surface of the void is equal to the dislocation core radius ρ_0 . The corresponding stress required to emit the dislocation is

$$\sigma_{cr} = \frac{Gb/a}{4\pi(1-\nu)} \left(\frac{r_0^2}{a^2} \frac{1}{f_0} - 2f_0 \right) + \frac{G\eta\zeta/\pi}{\zeta^2 + (\rho_0/b)^2} \frac{r_0^3}{a^3} \frac{1}{g_0}, \quad (16)$$

where f_0 is given by (9), and

$$g_0 = \sin \theta \left(1 - \frac{a^2}{r_0^2} \sin^2 \theta \right)^{1/2}. \quad (17)$$

The angle $\theta = \theta_{cr}$ at which the dislocation is emitted corresponds to the minimum value of the applied stress, σ_{cr}^{\min} , which is calculated numerically. The results are shown in Fig. 7. The critical stress for the emission of dislocation is significantly increased by the ledge creation. This is so because the ledge exerts a strong retarding force on the dislocation near the void, attracting it back to the surface of the void, regardless of the angle θ . The value $\eta = 0.2$, used to obtain one of the curves in Fig. 7, corresponds to a single crystal of copper at the shock temperature of 500 °C. The shear modulus of copper is $G = 40$ GPa, and the Poisson ratio is taken to be $\nu = 1/3$. The magnitude of the Burgers vector of $\{111\} \langle 110 \rangle$ dislocation is 0.255 nm, with its edge component $b = 0.22$ nm ($= 0.255$ nm $\times \sqrt{3}/2$). The surface energy of copper at 773 K is estimated⁶ to be $\gamma_{773} = 1.75$ J/m².

In the limit of very large voids,

$$\sigma_{cr} = \frac{G/\pi}{\sin 2\theta} \left[\frac{b/\rho_0}{4(1-\nu)} + \frac{2\eta\zeta}{\zeta^2 + (\rho_0/b)^2} \right], \quad a \gg b. \quad (18)$$

⁶ The surface energy of solids decreases with the temperature. For copper, this decrease is from $\gamma_0 = 1.79$ J/m² at 0 K (Rice, 1992) to $\gamma_m = 1.72$ J/m² at the melting temperature $T_m = 1357$ K (Porter and Easterling, 113, 2004). If a linear interpolation is used, the surface energy at the room temperature is $\gamma_{298} = 1.775$ J/m², while $\gamma_{773} = 1.75$ J/m². The parameter η is also temperature dependent, and this dependence can be deduced from the temperature dependence of γ , G and b via the relationship $\gamma = \eta Gb$.

This has the minimum value

$$\sigma_{cr}^{min} = \frac{G}{\pi} \left[\frac{b/\rho_0}{4(1-\nu)} + \frac{2\eta\zeta}{\zeta^2 + (\rho_0/b)^2} \right], \quad a \gg b, \tag{19}$$

corresponding to dislocation emission at $\theta_{cr} = 45^\circ$. Since

$$\frac{\zeta}{\zeta^2 + (\rho_0/b)^2} \approx 0.372 \frac{b}{\rho_0},$$

the critical stress (19) can also be written as

$$\sigma_{cr}^{min} = \frac{Gb}{\pi\rho_0} \left[\frac{1}{4(1-\nu)} + 0.744\eta \right], \quad a \gg b. \tag{20}$$

3. Biaxial loading conditions

A cylindrical void of radius a in an infinitely extended material, subjected to remote biaxial state of stress $\sigma_x = k\sigma$ and $\sigma_y = \sigma$ is shown in Fig. 8. For applied equal biaxial stress: $\sigma_x = \sigma_y$, $k = 1$; for uniaxial applied stress: $\sigma_x = 0$, $k = 0$; for the applied shear state of stress: $\sigma_x = -\sigma_y$, $k = -1$; for inplane uniaxial remote strain: $\epsilon_x = 0$, $k = \nu/(1-\nu)$ (equal to $1/2$ if $\nu = 1/3$). The elastic stress field around the void is

$$\begin{aligned} \sigma_r &= \frac{\sigma}{2} \left[(1+k) \left(1 - \frac{a^2}{r^2} \right) - (1-k) \left(1 - 4\frac{a^2}{r^2} + 3\frac{a^4}{r^4} \right) \cos 2(\phi + \varphi) \right], \\ \sigma_\varphi &= \frac{\sigma}{2} \left[(1+k) \left(1 + \frac{a^2}{r^2} \right) + (1-k) \left(1 + 3\frac{a^4}{r^4} \right) \cos 2(\phi + \varphi) \right], \\ \sigma_{r\varphi} &= \frac{\sigma}{2} (1-k) \left(1 + 2\frac{a^2}{r^2} - 3\frac{a^4}{r^4} \right) \sin 2(\phi + \varphi). \end{aligned} \tag{21}$$

The polar coordinates r and φ can be expressed in terms of the polar coordinates ρ and θ , emanating from the surface of the void (Fig. 8), by using the relationship (2). The angle ϕ specifies the intersection of the slip plane with the surface of the void, and is one of the unknowns in the analysis of the dislocation emission under biaxial loading conditions. The shear stress

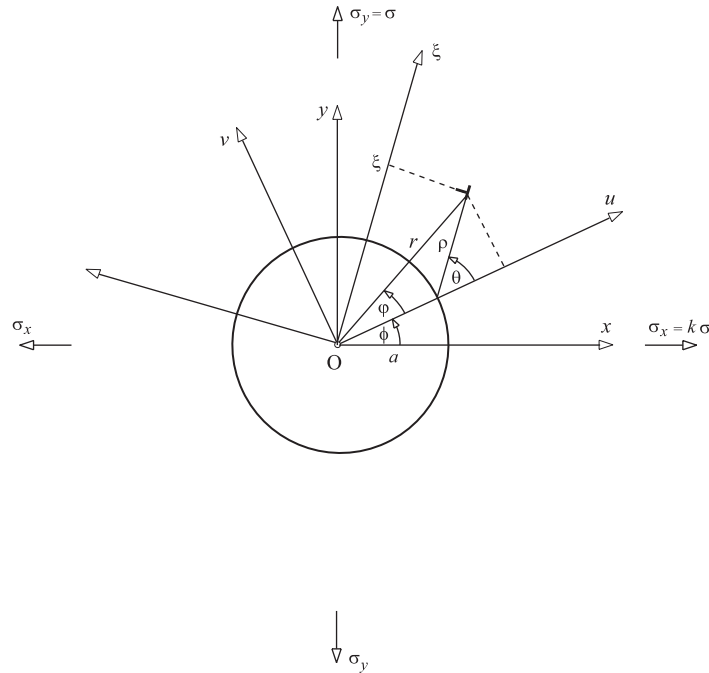


Fig. 8. A positive edge dislocation emitted from the surface of the void under remote biaxial state of stress. The angle ϕ specifies the intersection of the slip plane with the surface of the void. The slip plane is at the angle $\phi + \theta$ relative to the horizontal x -direction.

$\tau^a = \sigma_{\rho\theta}$ along the slip plane of the dislocation, induced by the applied loading, is determined from (21) by using the transformation

$$\tau^a = -\frac{1}{2}(\sigma_r - \sigma_\phi) \sin 2(\theta - \varphi) + \sigma_{r\varphi} \cos 2(\theta - \varphi). \quad (22)$$

This gives

$$\tau^a = \sigma \frac{ha^2}{2r^2}, \quad (23)$$

where a non-dimensional parameter $h = h(\rho, \theta, \phi)$ is defined by

$$h = (1 - k) \frac{r^2}{a^2} \sin 2(\theta + \phi) + (1 + k) \sin 2(\theta - \varphi) + (1 - k) \left(3 \frac{a^2}{r^2} - 2 \right) \sin 2(\theta - 2\varphi - \phi). \quad (24)$$

The corresponding Peach–Koehler force on the dislocation is

$$F^a = \tau^a b = \sigma b \frac{a^2}{2r^2} h(\rho, \theta, \phi). \quad (25)$$

It is noted that the hoop stress around the void ($r = a$) due to applied stress is $\sigma_\phi = \sigma[1 + k + 2(1 - k) \cos 2\phi]$, which is obtained from the second equation in (21) by taking $r = a$ and $\varphi = 0$. The corresponding maximum shear stress at the surface of the void is $\tau_{\max} = \sigma_\phi/2$. For positive σ , the hoop stress has the maximum value $\sigma_\phi^{\max} = (3 - k)\sigma$ at $\phi = 0$, if $k < 1$, and $\sigma_\phi^{\max} = (3k - 1)\sigma$ at $\phi = \pm\pi/2$, if $k > 1$. Also, it is noted that (21) delivers the stress distribution corresponding to the uniaxial loading $\sigma_x \neq 0$, $\sigma_y = 0$ by performing the limit $k \rightarrow \infty$ and $\sigma \rightarrow 0$, such that $\sigma k \rightarrow \sigma_x$. The resulting stress field is

$$\begin{aligned} \sigma_r &= \frac{\sigma_x}{2} \left[1 - \frac{a^2}{r^2} + \left(1 - 4 \frac{a^2}{r^2} + 3 \frac{a^4}{r^4} \right) \cos 2(\phi + \varphi) \right], \\ \sigma_\phi &= \frac{\sigma_x}{2} \left[1 + \frac{a^2}{r^2} - \left(1 + 3 \frac{a^4}{r^4} \right) \cos 2(\phi + \varphi) \right], \\ \sigma_{r\varphi} &= -\frac{\sigma_x}{2} \left(1 + 2 \frac{a^2}{r^2} - 3 \frac{a^4}{r^4} \right) \sin 2(\phi + \varphi). \end{aligned} \quad (26)$$

3.1. An analysis of the dislocation emission

The total glide force of the dislocation, driving it out of the void, is $F = F^a + F^i$, where the image force F^i exerted by the surface of the void is given by (4). Thus, by adding (4) and (25),

$$F = \sigma b \frac{a^2}{2r^2} h(\rho, \theta, \phi) + \frac{Gb^2 \cos(\theta - \varphi)}{2\pi(1 - \nu)} \frac{a^2}{r^3} \left(2 \frac{r^2 - a^2}{r^2} \sin^2 \theta - \frac{r^2}{a^2} \frac{r^2}{r^2 - a^2} \right). \quad (27)$$

Adopting the same criterion as in Section 2.2, the substitution of $\rho = \rho_0$ in the equilibrium condition $F = 0$ specifies the stress required to emit the dislocation from the surface of the void. This is

$$\sigma_{cr} = \frac{Gb/a}{2\pi(1 - \nu)} \frac{\sin 2(\theta - \varphi)}{h} \left(\frac{r_0^2}{a^2} \frac{1}{f_0} - 2f_0 \right), \quad (28)$$

where $\sin(\theta - \varphi) = a \sin \theta / r$, and f_0 is specified by (9).

The non-dimensional parameter $h = h(\rho_0, \theta, \phi)$ can be conveniently rewritten from (24) as

$$\begin{aligned} h &= (1 - k) \left[\frac{r_0^2}{a^2} - \left(3 \frac{a^2}{r_0^2} - 2 \right) \cos 4(\theta - \varphi_0) \right] \sin 2(\theta + \phi) + (1 + k) \left[\left(3 \frac{a^2}{r_0^2} - 2 \right) \sin 4(\theta - \varphi_0) \right] \cos 2(\theta + \phi) \\ &\quad + (1 + k) \sin 2(\theta - \varphi_0), \end{aligned} \quad (29)$$

so that the angle ϕ appears in the combination $2(\theta + \phi)$ only. The coordinates r_0 and φ_0 are specified by (2) with $\rho = \rho_0$. If σ is positive, the parameter h in (28) must also be positive. Table 2 lists this critical stress σ_{cr}^{\min} , and the angles ϕ_{cr} and θ_{cr} which

Table 2

The critical stress required for the dislocation emission under different biaxial loading conditions. In all four cases, $a = 5b$, $\rho_0 = b$, and $\nu = 1/3$. If $\nu \neq 1/3$, the listed values for σ_{cr}^{\min} should be multiplied by $2/[3(1 - \nu)]$.

	$k = 1$	$k = 1/2$	$k = 0$	$k = -1$
σ_{cr}^{\min}/G	0.166	0.143	0.126	0.101
ϕ_{cr} (°)	Any value	−9.8°	−10.5	−11.3
θ_{cr} (°)	54.5	56.0	57.1	58.8

specify the location and the direction of the dislocation emission from the surface of the void. The remote pure shear loading ($k = -1$) emits the dislocation most easily ($\sigma_{cr}^{min} = 0.101G$), because the stress concentration at the surface of the void is in this case the greatest (equal to 4). In the case of equal biaxial loading ($k = 1$), the stress concentration is only 2, and a significantly greater remote stress ($\sigma_{cr}^{min} = 0.166G$) is required for the dislocation emission.

In retrospect, note that the critical stress σ_{cr} in (28) depends on the angle ϕ only through the ϕ -dependence of the function h given by (29). Thus, the minimum value of σ_{cr} is associated with the maximum value of the function $h(\theta, \phi)$ with respect to ϕ . The condition $\partial h / \partial \phi = 0$ then gives

$$\tan 2(\theta + \phi) = \frac{r_0^2/a^2 - (3a^2/r_0^2 - 2) \cos 4(\theta - \phi_0)}{(3a^2/r_0^2 - 2) \sin 4(\theta - \phi_0)}. \tag{30}$$

This can be substituted into (29), so that h becomes a function of θ only. The angle θ_{cr} is the angle which maximizes such h . Having determined θ_{cr} , the angle ϕ_{cr} follows from (30).

Fig. 9 shows the variation of σ_{cr}^{min} with a/b for the four selected values of the loading parameter k , in the case $\rho_0 = b$. Fig. 10 shows the corresponding variation of the angles θ_{cr} and ϕ_{cr} with a/b . In the limit of very large voids ($\alpha \gg 1$), one has

$$\sigma_{cr} = \frac{Gb/\rho_0}{2\pi(1-\nu)} \frac{1}{h}, \quad h = [1 + k + 2(1 - k) \cos 2\phi] \sin 2\theta. \tag{31}$$

For $k \leq 1$, this has the minimum value

$$\sigma_{cr}^{min} = \frac{Gb/\rho_0}{2\pi(1-\nu)} \frac{1}{3-k}, \quad \theta_{cr} = \pi/4, \quad \phi_{cr} = 0, \tag{32}$$

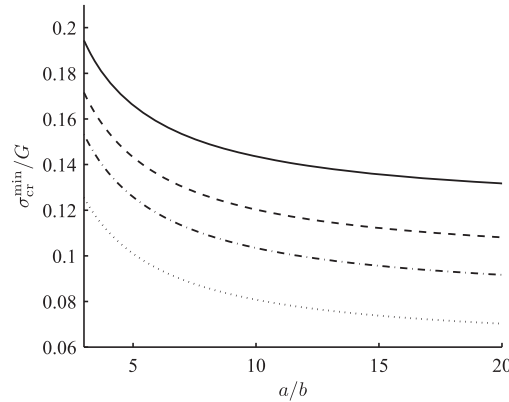


Fig. 9. The critical stress σ_{cr}^{min}/G vs. the void size a/b under combined loading in the case $\rho_0 = b$. The solid curve is for $k = 1$, the dashed curve is for $k = 1/2$, the dotted-dashed curve is for $k = 0$, and the dotted curve is for $k = -1$.

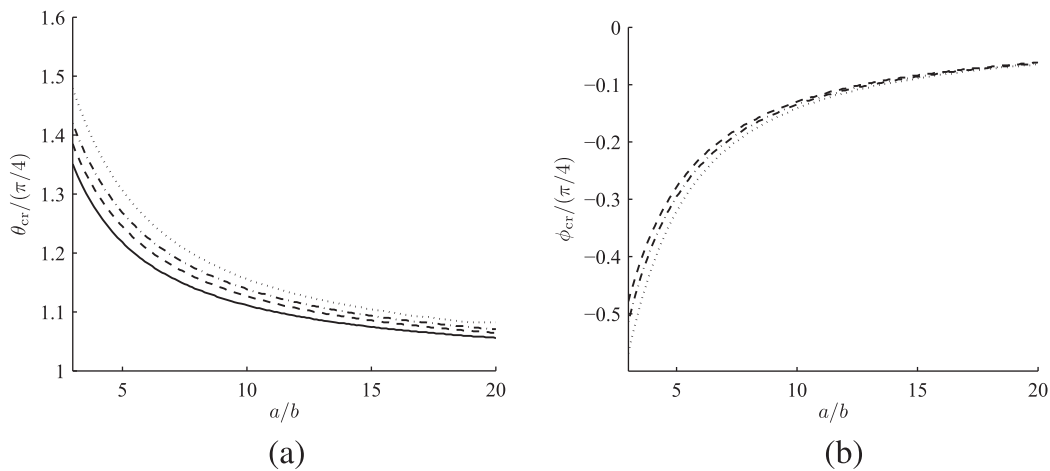


Fig. 10. The critical angles θ_{cr} and ϕ_{cr} (scaled by $\pi/4$) vs. the void size a/b under combined loading in the case $\rho_0 = b$. The solid curve is for $k = 1$, the dashed curve is for $k = 1/2$, the dotted-dashed curve is for $k = 0$, and the dotted curve is for $k = -1$. In the case $k = 1$, the angle ϕ_{cr} can be any angle, independently of a/b .

while for $k \geq 1$,

$$\sigma_{cr}^{min} = \frac{Gb/\rho_0}{2\pi(1-\nu)} \frac{1}{3k-1}, \quad \theta_{cr} = \pi/4, \quad \phi_{cr} = \pm\pi/2. \tag{33}$$

For the considerations in Section 4, which is concerned with the lattice orientation effects, we note that in the case of the uniaxial loading along the x -axis ($\sigma_x = \sigma, \sigma_y = 0$), the critical stress is given by (28) with the function h defined by

$$h = -\left[\frac{r_0^2}{a^2} - \left(3\frac{a^2}{r_0^2} - 2\right) \cos 4(\theta - \varphi_0)\right] \sin 2(\theta + \phi) - \left[\left(3\frac{a^2}{r_0^2} - 2\right) \sin 4(\theta - \varphi_0)\right] \cos 2(\theta + \phi) + \sin 2(\theta - \varphi_0). \tag{34}$$

The minimum value $\sigma_{cr}^{min} = 0.126G$ corresponds to $\phi_{cr} = 79.5^\circ$ and $\theta_{cr} = 57.1^\circ$, in agreement with the case $k = 0$ from Table 2 (uniaxial loading along the y -direction), the two critical angles ϕ_{cr} being the 90° complements of each other (Fig. 11). The stress concentration at the surface of the void in the first case is at $\phi = 0^\circ$, and in the second case at $\phi = \pm\pi/2$.

4. Lattice orientation effects

In this section, we determine the critical stress required to emit the dislocation along a particular slip plane within a single crystal available for the dislocation glide. Four $\{111\}$ slip planes of an fcc crystal are shown in Fig. 12a. Consider a straight dislocation along $[1\bar{1}0]$ direction, having the Burgers vector of the magnitude $a_0/\sqrt{2}$ in the direction $[0\bar{1}1]$, where a_0 is the lattice parameter of the crystalline lattice. The edge component of this dislocation is in the direction $[\bar{1}\bar{1}2]$, with the

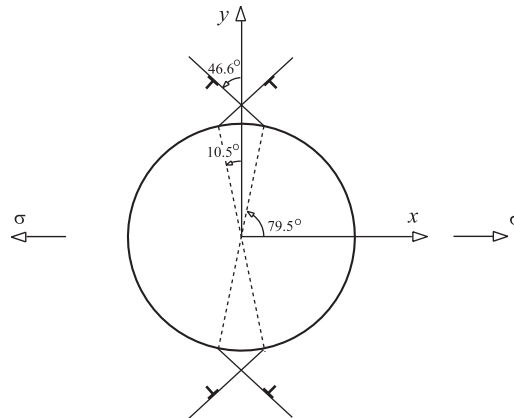


Fig. 11. Dislocation emission under uniaxial loading in the case $a = 5b, \rho_0 = b$, and $\nu = 1/3$. Each of the four shown dislocations are emitted under the stress $\sigma_{cr} = 0.126G$.

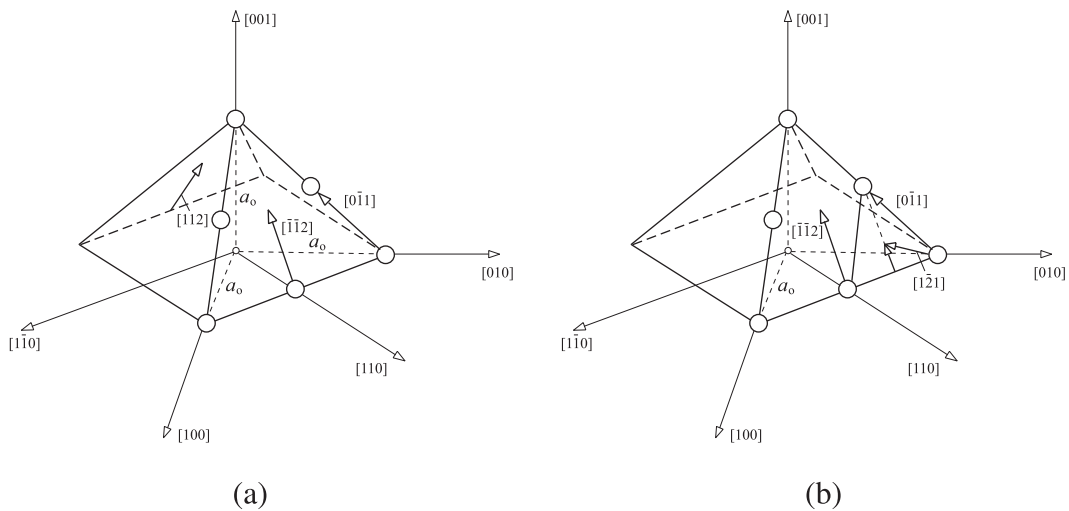


Fig. 12. (a) Four $\{111\}$ slip planes of an fcc crystal, with atoms shown schematically for one of the planes only. The Burgers vector $(a_0/2)[0\bar{1}1]$ of the dislocation line along $[1\bar{1}0]$ direction has the edge component of magnitude $(a_0/\sqrt{2}) \sin 60^\circ$ in the $[\bar{1}\bar{1}2]$ direction. (b) The Burgers vector of the partial dislocation is $(a_0/6)[1\bar{2}1]$, with its edge component $(a_0/12)[\bar{1}\bar{1}2]$.

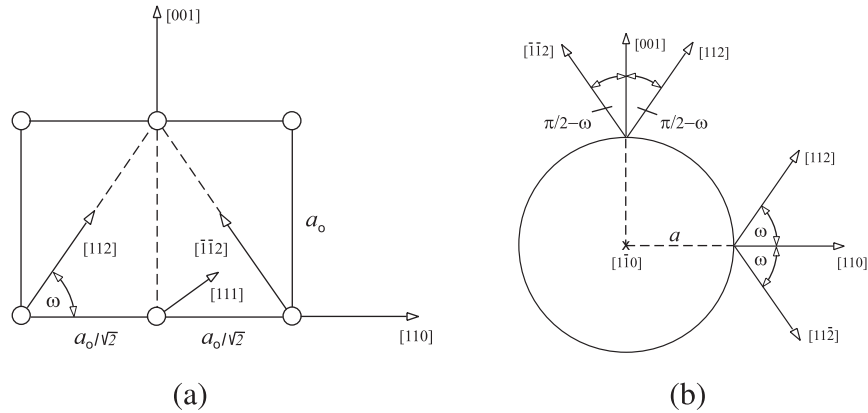


Fig. 13. (a) The mid-section of the lattice shown in Fig. 12a, within the plane spanned by $[1\ 1\ 0]$ and $[0\ 0\ 1]$ directions. The normal distance between the two slip planes is $d = (a_0/\sqrt{2}) \sin \omega = a_0/\sqrt{3}$, where $\tan \omega = \sqrt{2}$. (b) The cylindrical void with the axis in the $[1\ \bar{1}\ 0]$ direction. The edge components of two dislocations are along $(1\ 1\ 2)$ directions.

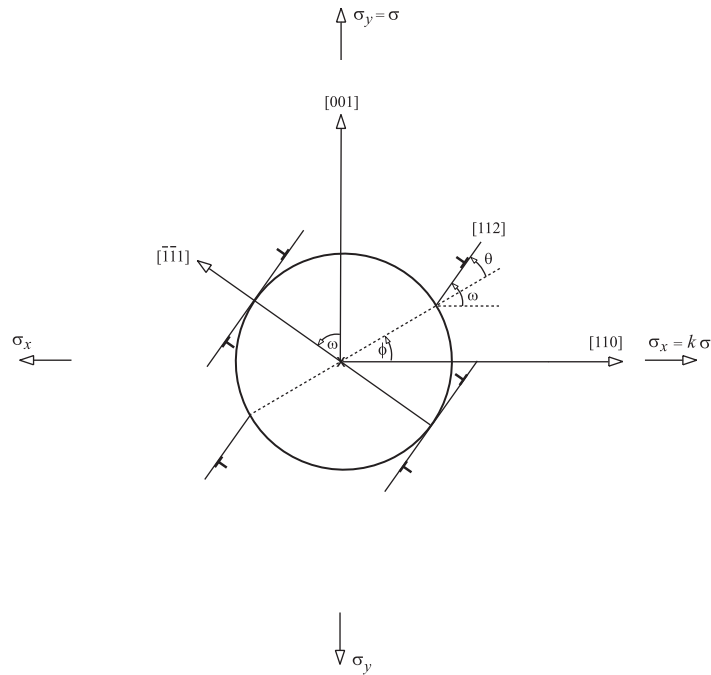


Fig. 14. A slip direction $[1\ 1\ 2]$ emanating from the surface of the void at the point defined by the angle ϕ . The slip direction is at the angle ω relative to the $[1\ 1\ 0]$ direction. Two slip directions $[1\ 1\ 2]$, tangent to the void and with an effective dislocation loop on each, are also shown. The void is under biaxial remote loading. Infinite stress would be required to emit the dislocation along the slip planes tangent to the surface of the void (orthogonal to indicated $[\bar{1}\ \bar{1}\ 1]$ direction), because there is no shear stress along those directions at the surface of the void.

magnitude $(a_0/\sqrt{2}) \sin 60^\circ = \sqrt{6}a_0/4$. One third of this value $(a_0/2\sqrt{6})$ is the magnitude of the Burgers vector of the edge component $(a_0/12)[\bar{1}\ \bar{1}\ 2]$ of the partial dislocation $(a_0/6)[1\ 2\ 1]$. We are considering here only the emission of a single dislocation with the Burgers vector in the direction of the edge component of the leading partial dislocation.⁷ The extension of the analysis to address the emission of an extended dislocation, in which the leading partial dislocation $[1\ 2\ 1]/6$ is emitted first, leaving a faulted plane behind it, and then the trailing partial dislocation $[2\ 1\ \bar{1}]/6$ is emitted under increased external loading to complete the $[1\ 1\ 0]/2$ dislocation, is a worthwhile extension of the present analysis, particularly for fcc metals with a low stacking fault energy (such as Cu).⁸ For bcc metals such as Mo dislocations do not split into Shockley partials and a perfect

⁷ MD simulations by Bringa et al. (submitted for publication) also reveal that during the process of void growth in copper by emission of partial dislocations, in many cases the leading partial is not followed by the trailing partial, which results in a complex network of stacking faults left behind.

⁸ An analytical study of the emission of partial dislocations from the crack tip within the Rice–Thomson model has been performed by Anderson (1986). See also Lin et al. (1996).

dislocation $[111]/2$ is emitted. A comprehensive MD analysis of the void growth by dislocation emission in bcc metals has been recently reported by Rudd (2009).

The section of the lattice within the plane spanned by the $[110]$ and $[001]$ directions is shown in Fig. 13a. The cylindrical void whose axis is in the $[1\bar{1}0]$ direction is shown in Fig. 13b; the edge component of two dislocations are along the indicated $\langle 112 \rangle$ directions. Only two pairs of slip directions are shown in Fig. 13b. Suppose that the biaxial loading is applied along the $[110]$ and $[001]$ directions, and that the dislocation emission along the $[112]$ is considered (Fig. 14). The angle $\omega = \phi + \theta$

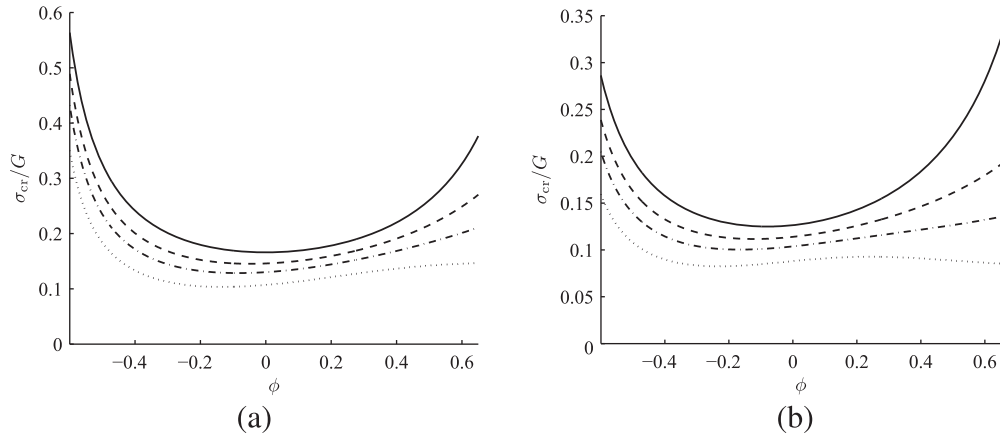


Fig. 15. (a) The variation of σ_{cr} with ϕ in the case of the loading specified by $k = 1$ (solid), $k = 1/2$ (dashed), $k = 0$ (dotted–dashed), and $k = -1$ (dotted curve); $a = 5b$ and $\rho_0 = b$. In each case the minimum value of σ_{cr} is the critical stress for the positive dislocation emission. The corresponding ϕ specifies the location of the emission. The opposite-signed dislocation would be emitted at the same ϕ under the opposite directed loading. (b) The same as in part (a), but with the core radius $\rho_0 = 1.5b$.

Table 3

The critical stress σ_{cr}^{min}/G and the angle ϕ_{cr} for the dislocation emission along the $[112]$ direction, under different loading conditions, for dislocations with the core radii $\rho_0 = b$ and $1.5b$. In all cases $a/b = 5$ and $\nu = 1/3$.

	$k = 1$	$k = 1/2$	$k = 0$	$k = -1$
$\rho_0 = b$				
σ_{cr}^{min}/G	0.166	0.145	0.128	0.104
ϕ_{cr} (°)	-0.1	-2.7	-4.9	-7.5
$\rho_0 = 1.5b$				
σ_{cr}^{min}/G	0.125	0.112	0.100	0.080
ϕ_{cr} (°)	-4.6	-6.9	-9.5	-13.2

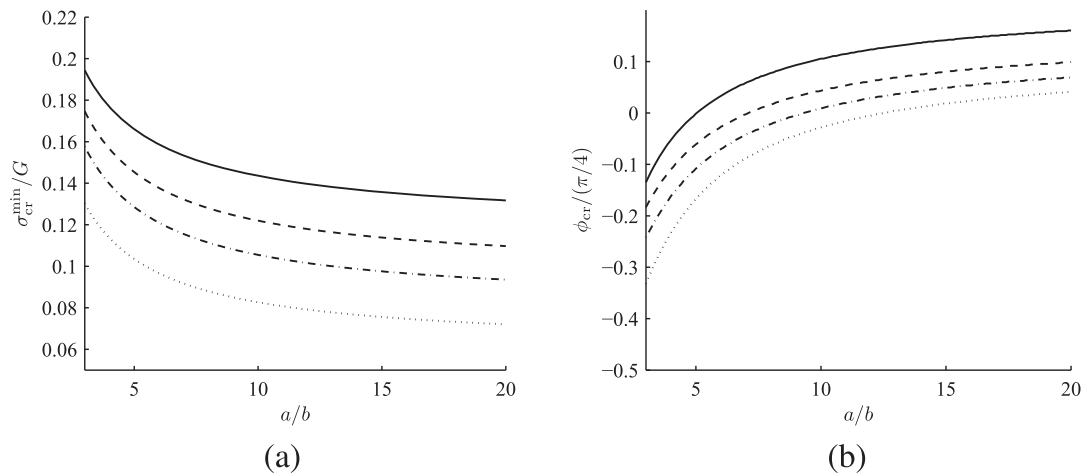


Fig. 16. (a) The variation of σ_{cr}^{min} with a/b in the case of the loading specified by $k = 1$ (solid), $k = 1/2$ (dashed), $k = 0$ (dotted–dashed), and $k = -1$ (dotted curve) in the case $\rho_0 = b$. (b) The corresponding variation of ϕ_{cr} .

Table 4

The critical stress σ_{cr}^{min}/G and the angle ϕ_{cr} for the dislocation emission along the [112] direction, under different loading conditions, for the void sizes $a = 3b$ and $10b$. In all cases $\rho_0 = b$ and $\nu = 1/3$.

	$k = 1$	$k = 1/2$	$k = 0$	$k = -1$
$a = 3b$				
σ_{cr}^{min}/G	0.194	0.175	0.158	0.130
ϕ_{cr} (°)	-6.1	-8.3	-10.9	-15.0
$a = 10b$				
σ_{cr}^{min}/G	0.144	0.122	0.106	0.083
ϕ_{cr} (°)	4.8	1.9	0.4	-1.3

Table 5

The critical stress σ_{cr}^{min}/G and the angle ϕ_{cr} for the dislocation emission along the [112] direction, under different loading conditions, for large voids $a \gg b$, and for $\rho_0 = b$ and $\nu = 1/3$.

$a \gg b$	$k = 1$	$k = 1/2$	$k = 0$	$k = -1$
σ_{cr}^{min}/G	0.1194	0.0971	0.0814	0.0614
ϕ_{cr} (°)	9.72	6.93	5.85	4.86(+90)

between the [110] and [112] directions is $\omega = 54.7^\circ$ ($\tan \omega = \sqrt{2}$), and therefore $\sin 2(\phi + \theta) = 2\sqrt{2}/3$ and $\cos 2(\phi + \theta) = -1/3$. When this is substituted into (29), the function h becomes

$$h = \frac{2\sqrt{2}}{3}(1 - k) \left[\frac{r_0^2}{a^2} - \left(3 \frac{a^2}{r_0^2} - 2 \right) \cos 4(\theta - \phi_0) \right] - \frac{1}{3}(1 - k) \left[\left(3 \frac{a^2}{r_0^2} - 2 \right) \sin 4(\theta - \phi_0) \right] + (1 + k) \sin 2(\theta - \phi_0), \quad (35)$$

where $\theta = \omega - \phi$. The required stress⁹ for the emission of the positive edge dislocation is obtained by minimizing the stress σ_{cr} in (28) with respect to ϕ , in the range $-\pi/2 + \omega \leq \phi \leq \pi/2 + \omega$. Fig. 15a shows the plots $\sigma_{cr} = \sigma_{cr}(\phi)$ for the four different loadings ($k = 1, 1/2, 0, -1$), in the case $a = 5b$ and $\rho_0 = b$.¹⁰ Table 3 lists the corresponding values of the critical stress σ_{cr}^{min} and the associated angle ϕ_{cr} . The remote pure shear loading ($k = -1$) emits the dislocation most easily ($\sigma_{cr} = 0.104G$). In the case of equal biaxial loading ($k = 1$), the stress concentration factor at the surface of the void is only one half of that from the pure shear loading, and the critical stress for the dislocation emission is $\sigma_{cr}^{min} = 0.166G$. Fig. 15b shows the same as part (a) of this figure, but for the dislocation core radius $\rho_0 = 1.5b$. By comparing the results listed in Table 3, it follows that less stress is required to emit the wider dislocations, and the emission is further away from the point of maximum stress concentration on the surface of the void (ϕ_{cr} more pronouncedly different from zero).

Fig. 16a shows the variation of σ_{cr}^{min} with a/b in the four considered loading cases, with $\rho_0 = b$. The corresponding variation of ϕ_{cr} is shown in Fig. 16b. Table 4 lists the specific values of the critical stress σ_{cr}^{min} and the associated angle ϕ_{cr} , for $a = 3b$ and $a = 10b$, which reveals that greater the radius of the void, smaller the stress required for the dislocation emission, and closer the emission of the dislocation from the point of the void with the maximum stress concentration factor ($\phi = 0$). In the limit of very large voids ($\alpha \gg 1$), one has

$$\sigma_{cr} = \frac{Gb/\rho_0}{2\pi(1 - \nu)} \frac{1}{h}, \quad h = [1 + k + 2(1 - k) \cos 2\phi] \sin 2(\omega - \phi), \quad (36)$$

which has the minimum at the angle ϕ which maximizes h . Table 5 lists the values of the critical stress σ_{cr}^{min}/G and the angle ϕ_{cr} for the dislocation emission along the [112] direction in the case $\rho_0 = b$, and $\nu = 1/3$. For different ρ_0/b and ν the tabulated values of σ_{cr}^{min}/G should be multiplied by $2b/[3(1 - \nu)\rho_0]$. For $k = 1$, the angle $\phi_{cr} = \omega - \pi/4$, $h_{max} = 2$, and $\sigma_{cr}^{min} = G(b/\rho_0)/[4\pi(1 - \nu)]$.

It should be noted that for smaller voids, there is only a set of few (discrete) slip planes emanating from the surface of the void (their distance being $d = a_0/\sqrt{3}$). The determination of the required stress for the dislocation emission based on the assumed continuous distribution of the slip planes and the condition $d\sigma_{cr}/d\phi = 0$ can then be interpreted as follows. If there is a dilute distribution of voids within a crystalline lattice, statistically there is always a void positioned relative to the lattice so that it is intersected by the slip plane at an arbitrary point on its surface; thus the condition $d\sigma_{cr}/d\phi = 0$. If a growth of a particular void is only considered, one can evaluate σ_{cr} for the discrete set of values of ϕ , corresponding to the actual slip planes,

⁹ The assumption of isotropy is adopted to proceed with the analytical study, because there is no closed form solution for a dislocation near the void in a cubic crystal or in an anisotropic material. A similar analysis of the crystal-orientation dependent evolution of edge dislocations from a void in a single crystal copper was used by Song et al. (2006) and Zhu et al. (2007). See also Kysar et al. (2005) and Gan et al. (2006).

¹⁰ The infinite value of σ_{cr} in the plots for some values of ϕ means that the shear stress due to applied loading at the location of the dislocation is there equal to zero, so that there is no driving force on the dislocation to overcome the image force from the surface of the void and the dislocation cannot be in equilibrium at $\rho = \rho_0$ at those values of ϕ .

and identify the minimum value among these by direct comparison. In this case, it may be reasonably expected that the slip plane which intersects the surface of the void in close proximity of the point of the greatest stress concentration due to applied loading is the critical slip plane along which the emission of the first dislocation will take place. An alternative approach to predict the onset and evolution of the growth or collapse of nanovoids is to employ the molecular dynamics based calculations (e.g., Dávila et al., 2005; Marian et al., 2005; Traiviratana et al., 2008). The calculations performed by Traiviratana et al. (2008) under remote uniaxial strain conditions predict the values of critical stress in good agreement with the results presented in this paper, particularly for larger voids (Table 6).

Table 6

The comparison of the critical stress σ_{cr}^{min}/G for the dislocation emission along the [112] direction in the case of the remote uniaxial strain from the present calculations (with $k = 1/2$, $\rho_0 = b$ and $\nu = 1/3$), and from the atomistic calculations for copper by Traiviratana et al. (2008). The critical stress in the second raw of the table is twice the value of the von Mises stress reported in their Fig. 4a.

σ_{cr}^{min}/G	$a/b = 4$	$a/b = 8$	$a/b = 16$
This paper	0.157	0.128	0.113
Atomistic calculation	0.147	0.124	0.100

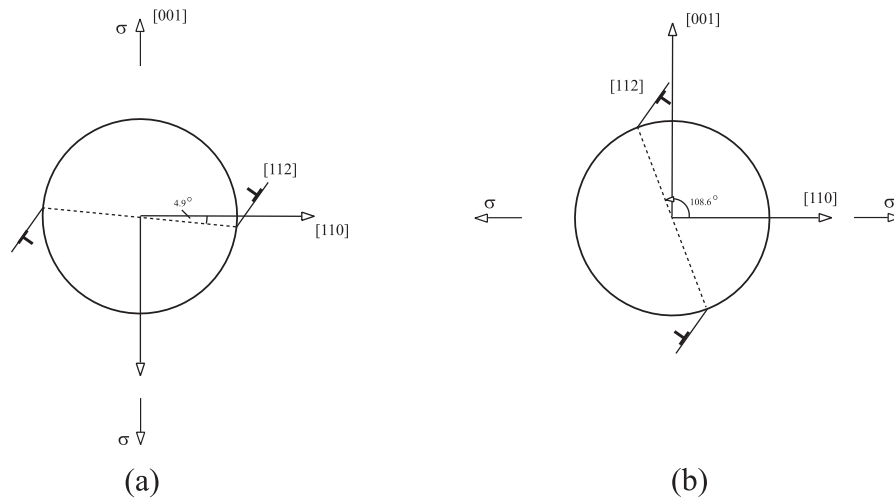


Fig. 17. Dislocation emission along the [112] direction in the case of uniaxial loading along the: (a) [001], and (b) [110] direction. The required stress for the dislocation emission in the first case is $\sigma_{cr} = 0.131G$, and in the second case $\sigma_{cr} = 0.128G$ (for $a/b = 5$, $\rho_0 = b$, and $\nu = 1/3$).

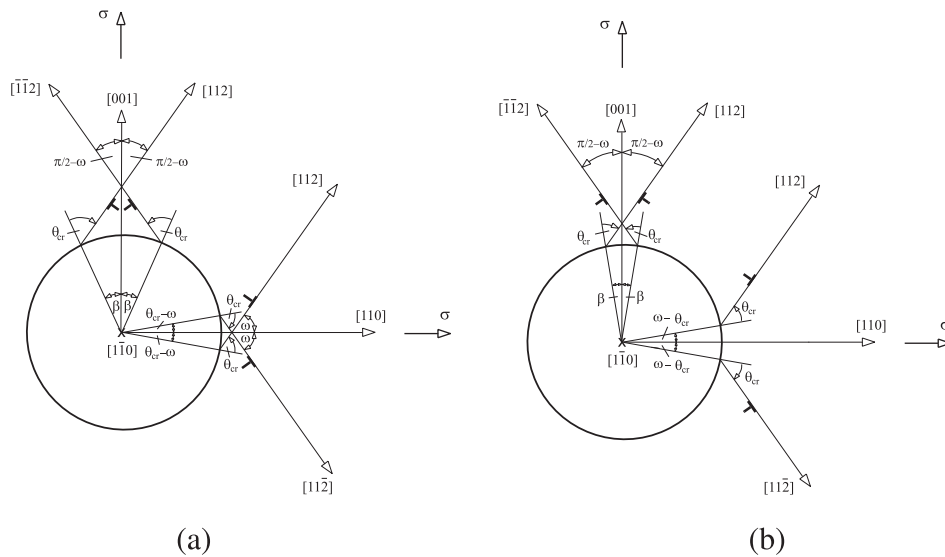


Fig. 18. Dislocation emission along the slip planes in the case: (a) $\theta_{cr} > \omega$, and (b) $\theta_{cr} < \omega$. In both cases, the angle $\beta = \theta_{cr} + \omega - \pi/2$.

and therefore their interaction and possible locking at the slip plane intersection become an important part of the analysis (Lubarda et al., 1993; Cleveringa et al., 1999; Lubarda, 2006). The interaction among dislocations may hinder or facilitate the emission, thus contributing to an increase or decrease of the threshold stress level required for the void growth. The details of this analysis are not given here, but the study is analogous to that presented by Lubarda et al. (2004), i.e., in the expression for the Peach–Koehler force on each dislocation the contribution from the shear stress produced by all other, or at least nearby dislocations needs to be included. Fig. 19 shows a plausible scenario of an isotropic void growth by emission of four dislocation dipoles along two pairs of $[11\bar{2}]$ and $[\bar{1}12]$ slip directions. It is assumed that dislocations arrived at the positions shown sequentially, one after another, avoiding their locking at the slip plane intersections. A quantitative analysis will be presented in a separate paper.

Acknowledgments

Research support from the Montenegrin Academy of Sciences and Arts and discussions with Dr. Eduardo Bringa are kindly acknowledged. Helpful comments and suggestions by reviewers are also acknowledged.

Appendix A. Stress field due to edge dislocation near a void

The stress state at an arbitrary point B due to edge dislocation with the Burgers vector $\mathbf{b} = \{b_\xi, b_\eta\}$ located at the point A near a circular void of radius a (Fig. A.1) is determined as follows. If the dislocation is created by the displacement discontinuity along the cut from the free surface of the void to the center of the dislocation, the Airy stress functions for the two dislocation components are (Lubarda, submitted for publication)

$$\chi^{b_\xi} = -\frac{Gb_\xi}{2\pi(1-\nu)} \left[z_1 \ln z_1 \sin \psi_1 - z_2 \ln z_2 \sin \psi_2 + \frac{\alpha^2 - 1}{2\alpha^3} a \left(\sin 2\psi_2 - \frac{\alpha^2 - 1}{\alpha} \frac{a}{z_2} \sin \psi_2 \right) \right], \quad (\text{A.1})$$

$$\chi^{b_\eta} = \frac{Gb_\eta}{2\pi(1-\nu)} \left[z_1 \ln z_1 \cos \psi_1 - z_2 \ln z_2 \cos \psi_2 - \frac{\alpha^2 - 1}{2\alpha^3} a \left(\cos 2\psi_2 - \frac{\alpha^2 - 1}{\alpha} \frac{a}{z_2} \cos \psi_2 + 2\alpha^2 \ln \frac{z_2}{a} \right) \right]. \quad (\text{A.2})$$

The Airy stress function for the whole dislocation is $\chi = \chi^{b_\xi} + \chi^{b_\eta}$, which delivers the stress components by

$$\sigma_\xi = \frac{\partial^2 \chi}{\partial \eta^2}, \quad \sigma_\eta = \frac{\partial^2 \chi}{\partial \xi^2}, \quad \sigma_{\xi\eta} = -\frac{\partial^2 \chi}{\partial \xi \partial \eta}. \quad (\text{A.3})$$

The nonsingular parts of the stress, giving rise to image force on the dislocation exerted by the surface of the void, are

$$\begin{aligned} \sigma_\xi &= -\frac{Gb_\eta}{2\pi(1-\nu)} \left(\frac{r^2 - a^2}{r^3} - \frac{a^2}{r} \frac{1}{r^2 - a^2} \right), \\ \sigma_\eta &= \frac{Gb_\eta}{2\pi(1-\nu)} \left(\frac{r^2 - a^2}{r^3} + \frac{a^2}{r} \frac{1 - 2r^2/a^2}{r^2 - a^2} \right), \\ \sigma_{\xi\eta} &= -\frac{Gb_\xi}{2\pi(1-\nu)} \frac{r}{r^2 - a^2}. \end{aligned} \quad (\text{A.4})$$

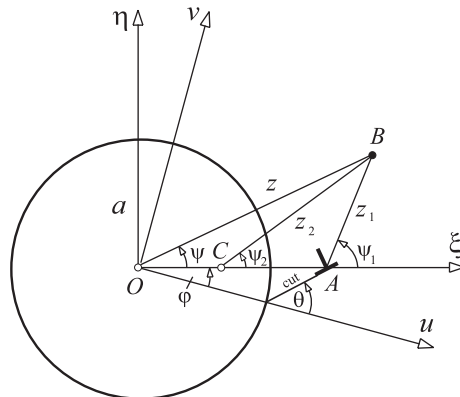


Fig. A.1. The radii z, z_1, z_2 and the angles ψ, ψ_1, ψ_2 appearing in the expressions for the Airy stress functions and the stress components at an arbitrary point B due to edge dislocation at the point A . The radius of the void is a , and the lengths $OA = r = \alpha a$ and $OC = a/\alpha$.

The shear stress along the slip of the dislocation is

$$\tau^i = \frac{1}{2}(\sigma_\eta - \sigma_\xi) \sin 2(\theta - \varphi) + \sigma_{z\eta} \cos 2(\theta - \varphi). \quad (\text{A.5})$$

Since $b_\xi = b \cos(\theta - \varphi)$, $b_\eta = b \sin(\theta - \varphi)$, where b is the magnitude of the Burgers vector of the dislocation, and since $\sin(\theta - \varphi) = (a/r) \sin \theta$, the substitution of (A.4) into (A.5) yields

$$\tau^i = \frac{Gb \cos(\theta - \varphi)}{2\pi(1 - \nu)} \frac{a^2}{r^3} \left(2 \frac{r^2 - a^2}{r^2} \sin^2 \theta - \frac{r^2}{a^2} \frac{r^2}{r^2 - a^2} \right). \quad (\text{A.6})$$

Thus, the image force on the dislocation ($F^i = b\tau^i$) is as given by expression (4) of the main text.

References

- Anderson, P.M., 1986. Ph.D. Thesis. Division of Applied Sciences, Harvard University, Cambridge, MA.
- Borg, U., Niordson, C.F., Kysar, J.W., 2008. Size effect on void growth in single crystals with distributed voids. *Int. J. Plast.* 24, 688–701.
- Bringa, E.M., Traiviratana, S., Meyers, M.A., submitted for publication. Void initiation in an fcc metal: molecular dynamics. *Acta Mater.*
- Clevering, H.H.M., Van der Giessen, E., Needleman, A., 1999. A discrete dislocation analysis of bending. *Int. J. Plast.* 15, 837–868.
- Cuitiño, A.M., Ortiz, M., 1996. Ductile fracture by vacancy condensation in fcc crystals. *Acta Mater.* 44, 427–436.
- Dávila, L.P., Erhart, P., Bringa, E.M., Meyers, M.A., Lubarda, V.A., Schneider, M.S., Becker, R., Kumar, M., 2005. Atomistic modeling of shock-induced void collapse in copper. *Appl. Phys. Lett.* 86. Article No. 161902.
- Dundurs, J., Mura, T., 1964. Interaction between an edge dislocation and a circular inclusion. *J. Mech. Phys. Solids* 12, 177–189.
- Farrissey, L., Ludwig, M., McHugh, P.E., Schmauder, S., 2000. An atomistic study of void growth in single crystalline copper. *Comput. Mater. Sci.* 18, 102–117.
- Fisher, F.D., Antretter, T., 2009. Deformation, stress state and thermodynamic force for a growing void in an elastic–plastic material. *Int. J. Plast.* 25, 1819–1832.
- Gan, Y.X., Kysar, J.W., Morse, T.L., 2006. Cylindrical void in a rigid-ideally plastic single crystal II: experiments and simulations. *Int. J. Plast.* 22, 39–72.
- Hirth, J.P., Lothe, J., 1982. *Theory of Dislocations*, second ed. Wiley, New York.
- Huang, Y., Qu, S., Hwang, K.C., Li, M., Gao, H., 2004. A conventional theory of mechanism-based strain gradient plasticity. *Int. J. Plast.* 21, 753–782.
- Huang, M., Li, Z., Wang, C., 2007. Discrete dislocation dynamics modelling of microvoid growth and its intrinsic mechanism in single crystals. *Acta Mater.* 55, 1387–1396.
- Hussein, M., Borg, U., Niordson, C.F., Deshpande, V.S., 2008. Plasticity size effects in voided crystals. *J. Mech. Phys. Solids* 56, 114–131.
- Kysar, J.W., Gan, Y.X., Mendez-Arzuza, G., 2005. Cylindrical void in a rigid-ideally plastic single crystal. Part I: anisotropic slip line theory solution for face-centered cubic crystals. *Int. J. Plast.* 21, 1481–1520.
- Li, Z., Steinmann, P., 2006. Rve-based studies on the coupled effects of void size and void shape on yield behavior and void growth at micron scales. *Int. J. Plast.* 22, 1195–1216.
- Lin, K.M., Lin, H.C., Chen, K.C., 1996. Extended dislocations around a semi-infinite crack. *Eng. Fract. Mech.* 54, 395–403.
- Liu, B., Huang, Y., Li, M., Hwang, K.C., Liu, C., 2005. A study of the void size effect based on the Taylor dislocation model. *Int. J. Plast.* 21, 2107–2122.
- Liu, B., Zhang, X.M., Tang, J.G., Du, Y.X., 2007. Simulation of void growth and coalescence behavior with 3D crystal plasticity. *Comput. Mater. Sci.* 40, 130–139.
- Lubarda, V.A., 1999. On the non-uniqueness of solution for screw dislocations in multiply connected regions. *J. Elasticity* 52, 289–292.
- Lubarda, V.A., 2006. Dislocation conditions revisited. *Int. J. Solids Struct.* 43, 3444–3458.
- Lubarda, V.A., Markenscoff, X., 2003. The stress field for a screw dislocation near cavities and straight boundaries. *Mater. Sci. Eng. A* 349, 327–334.
- Lubarda, V.A., Markenscoff, X., 2006. Variable core model and the Peierls stress for the mixed (screw-edge) dislocation. *Appl. Phys. Lett.* 89, 151923–151923-3.
- Lubarda, V.A., Markenscoff, X., 2007. Configurational force on a lattice dislocation and the Peierls stress. *Arch. Appl. Mech.* 77, 147–154.
- Lubarda, V.A., Blume, J.A., Needleman, A., 1993. An analysis of equilibrium dislocation distributions. *Acta Metall. Mater.* 41, 625–642.
- Lubarda, V.A., Schneider, M.S., Kalantar, D.H., Remington, B.R., Meyers, M.A., 2004. Void growth by dislocation emission. *Acta Mater.* 52, 1397–1408.
- Lubarda, V.A., submitted for publication. Image force on a straight dislocation emitted from a circular void.
- Marian, J., Knap, J., Ortiz, M., 2005. Nanovoid deformation in aluminum under simple shear. *Acta Mater.* 53, 2893–2900.
- Meyers, M.A., Traiviratana, S., Lubarda, V.A., Bringa, E.M., Benson, D.J., 2009. The role of dislocations in the growth of nanosized voids in ductile failure of metals. *J. Mater.* 61, 35–41.
- Nabarro, F.R.N., 1997. Theoretical and experimental estimates of the Peierls stress. *Philos. Mag. A* 75, 703–711.
- Ohashi, T., 2005. Crystal plasticity analysis of dislocation emission from microvoids. *Int. J. Plast.* 21, 2071–2088.
- Porter, D.A., Easterling, K.E., 2004. *Phase Transformations in Metals and Alloys*, second ed. Taylor & Francis, New York. p. 113.
- Potirniche, G.P., Hearndon, J.L., Horstemeyer, M.F., Ling, X.W., 2006a. Lattice orientation effects on void growth and coalescence in fcc single crystals. *Int. J. Plast.* 22, 921–942.
- Potirniche, G.P., Horstemeyer, M.F., Wagner, G.J., Gullett, P.M., 2006b. A molecular dynamics study of void growth and coalescence in single crystal nickel. *Int. J. Plast.* 22, 257–278.
- Quinn, D., Connolly, P., Howe, M., McHugh, P., 1995. Simulation of void growth in WC–Co hardmetals using crystal plasticity theory. *Int. J. Mech. Sci.* 39, 173–183.
- Rice, J.R., 1992. Dislocation nucleation from a crack tip: an analysis based on the Peierls concept. *J. Mech. Phys. Solids* 40, 239–271.
- Rice, J.R., Thomson, R., 1974. Ductile versus brittle behaviour of crystals. *Philos. Mag. A* 29, 73–97.
- Rudd, R.E., 2009. Void growth in bcc metals simulated with molecular dynamics using the Fennis–Sinclair potential. *Philos. Mag.* 89, 3133–3161.
- Rudd, R.E., Belak, J.F., 2002. Void nucleation and associated plasticity in dynamic fracture of polycrystalline copper: an atomistic simulation. *Comput. Mater. Sci.* 24, 148–153.
- Rudd, R.E., Seppälä, E.T., Dupuy, L.M., Belak, J., 2007. Void coalescence processes quantified through atomistic and multiscale simulation. *J. Comput.-Aided Mater. Des.* 14, 425–434.
- Segurado, J., Llorca, J., 2009. An analysis of the size effect on void growth in single crystals using discrete dislocation dynamics. *Acta Mater.* 57, 1427–1436.
- Segurado, J., Llorca, J., 2010. Discrete dislocation dynamics analysis of the effect of lattice orientation on void growth in single crystals. *Int. J. Plasticity* 26, 806–819.
- Seppälä, E.T., Belak, J., Rudd, R.E., 2004. Effect of stress triaxiality on void growth in dynamic fracture of metals: a molecular dynamics study. *Phys. Rev. B* 69, 134101-1–134101-19.
- Song, Z.-F., Zhu, W.-J., Deng, X.-L., He, H.-L., 2006. Crystal-orientation dependent evolution of edge dislocations from a void in single crystal Cu. *Chin. Phys. Lett.* 23, 3041–3044.
- Timoshenko, S.P., Goodier, J.N., 1970. *Theory of Elasticity*, third ed. McGraw-Hill, New York.
- Traiviratana, S., Bringa, E.M., Benson, D.H., Meyers, M.A., 2008. Void growth in metals: atomistic simulations. *Acta Mater.* 56, 3874–3886.

- Tvergaard, V., 1990. Material failure by void growth to coalescence. *Adv. Appl. Mech.* 27, 83–151.
- Tvergaard, V., Niordson, C., 2004. Nonlocal plasticity effects on interaction of different size voids. *Int. J. Plast.* 20, 107–120.
- Wen, J., Huang, Y., Hwang, K.C., Liu, C., Li, M., 2005. The modified Gurson model accounting for the void size effect. *Int. J. Plast.* 21, 381–395.
- Wolfer, W.G., Drugan, W.J., 1988. Elastic interaction between a prismatic dislocation loop and a spherical cavity. *Philos. Mag. A* 57, 923–937.
- Zhu, W.-J., Song, Z.-F., Deng, X.-L., He, H.-L., Cheng, X., 2007. The effect of lattice orientation on the nanovoid growth in copper under shock loading. *Phys. Rev. B* 75, 024104-1–024104-5.